NANO LETTERS

pubs.acs.org/NanoLett Letter

Engineering Twins within Lattice-Matched Co/CoO Heterostructure Enables Efficient Hydrogen Evolution Reactions

Taili Yang, Yaotian Yan,* Ruonan Liu, Keke Huang, Rongrong Xu, Jiping Chen, Jinchun Tu, Shude Liu,* Ling Kang,* Zixuan Wang, Jian Cao, and Junlei Qi*

Cite This: https://doi.org/10.1021/acs.nanolett.5c00472 Read Online

ACCESS | Metrics & More | Article Recommendations | Supporting Information

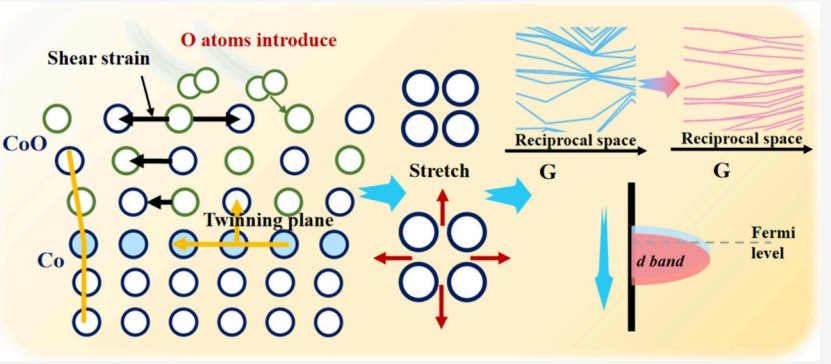

ABSTRACT: Twinning, as an effective strain engineering strategy, has demonstrated significant potential in modifying cost-effective transition metal electrocatalysts. However, controllable construction and structure−activity relationships of twinning in electrocatalysts remain formidable challenges. Here, we engineered a lattice-matched Co/CoO heterostructure with enriched twin boundaries through flash Joule heating, where the twins form via lattice matching within homogeneous space groups. XAFS analysis reveals significantly reduced Co coordination numbers in the heterostructure, indicating substantial atomic displacement from the equilibrium positions. The coherent twinning interfaces induce trapped strain, downshifting the d-band center by 0.4 eV and flattening bands near the Fermi level, optimizing the electronic structure for the hydrogen evolution reaction. Consequently, the engineered heterostructure exhibits exceptional performance with an ultralow overpotential of 49 mV at 10 mA cm^{-2} in alkaline media and remarkable stability over 500 h. Notably, the water splitting can be driven with an ultralow cell voltage of 2.05 V at 1 A cm^{-2}.

KEYWORDS: *twins, lattice match, thermal shock, lattice distortions, hydrogen evolution reaction*

The accelerating global energy crisis and environmental concerns have intensified the pursuit of sustainable and clean energy technologies. Water electrolysis for hydrogen production represents a promising avenue, offering an environmentally benign approach to storing renewable energy in chemical bonds. However, the high cost and limited availability of noble metals, commonly used in commercial electrocatalysis, restrict their widespread application in the clean energy field.[1−7] Hence, the development of affordable, efficient, and stable nonprecious metal electrocatalysts has emerged as a crucial issue in this area.

Transition metal-based catalysts show promise for water splitting due to their malleable structural attributes, commendable stability, and substantial storage capacity.[8−10] These catalysts include oxides,[11] phosphides,[12] LDHs,[13] MOFs,[14] and their respective composites. Among them, Co-based catalysts, such as Co_3O_4,[15] CoP,[16,17] and CoS,[18] offer advantages in natural abundance and unique physicochemical properties. However, transition metal compounds typically show suboptimal hydrogen binding energies. Integrating the superior electrical conductivity of metals with the hydrogen adsorption affinity of transition metal compounds is an effective strategy that can modulate the adsorption and desorption kinetics of intermediates through strain and coupling effects, thereby optimizing the catalytic activity. For instance, Zhu et al.[19] have reported the epitaxial Co−Ni_3N heterostructures, which facilitated electron transfer across different structural domains at the epitaxial interface, leading to a significant enhancement in catalytic activity for both hydrogen and oxygen evolution reactions. However, conventional heterostructures often

Received: January 21, 2025
Revised: April 14, 2025
Accepted: April 15, 2025

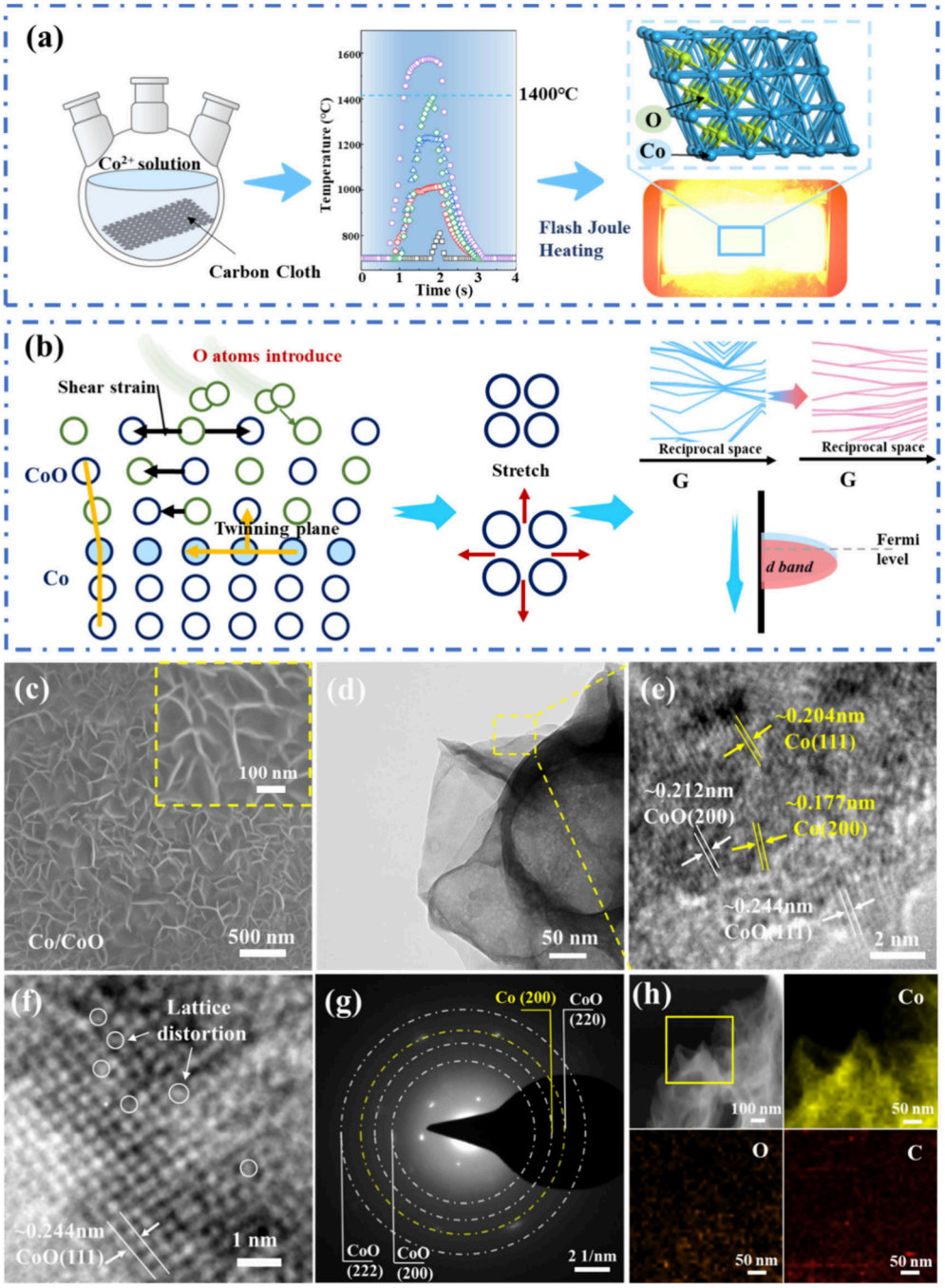

Figure 1. (a) Schematic diagram of the preparation of Co/CoO. (b) Schematic diagram of the lattice-matched Co/CoO heterostructures-induced twins. Structural characterization of Co/CoO nanosheets. (c) The SEM image of Co/CoO. (d) The TEM image of Co/CoO. (e, f) High resolution TEM of Co/CoO. (g) SAED pattern of Co/CoO. (h) EDS elemental mappings of Co, O, and C.

exhibit substantial differences in crystalline phases, and traditional modification methods based on elemental tuning have reached a bottleneck. This situation highlights the ongoing challenge in the design of lattice-matched heterostructures to overcome these limitations.

Twin boundaries are generated when two separate crystals share a common subset of lattice points symmetrically, resulting in the intricate interplay of growth between the two distinct crystalline entities in a variety of specific crystallographic orientations. Such twinning interfaces can significantly alter the intrinsic material properties, including but not limited to the enhancement of mechanical robustness and the augmentation of thermal resilience. Song et al.[20] demonstrated that rational interface engineering in electrospun nanomaterials enables strong electronic interactions between distinct phases within heterostructures, significantly enhancing active site density and charge transfer efficiency, thereby improving electrocatalytic performance for water splitting. Ye et al.[21] revealed that Co and CoO heterojunctions rich in oxygen vacancies, introduced via O plasma treatment, significantly enhanced activity by modulating the surface electronic structure, increasing defect density, and promoting charge transfer kinetics in zinc−air battery systems. The formation of twin boundaries leads to variations in interatomic distances,

https://doi.org/10.1021/acs.nanolett.5c00472
Nano Lett. XXXX, XXX, XXX−XXX

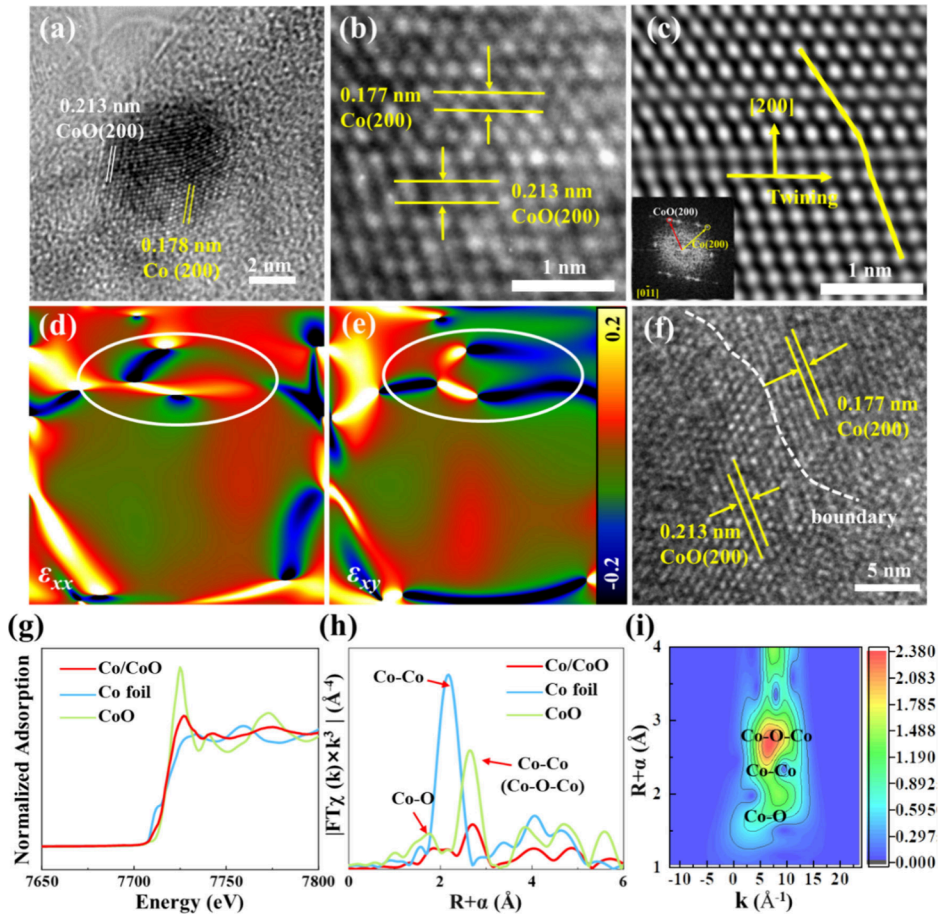

Figure 2. (a, b) HRTEM image of Co/CoO. (c) IFFT patterns of (111) and (200) planes. (d, e) Strain distributions of ε_{xx} and γ_{xy}. (f) HRTEM image of CoO@Co. (g) Normalized XANES spectra at the Co K-edge. (h) Fourier-transformed EXAFS spectra. (i) Wavelet transform analysis for the Co K-edge of Co/CoO.

which in turn affect the overlapping distribution of electronic energy bands, demonstrating a unique potential that surpasses the limitations of conventional elemental modulation. It is noteworthy that the d-band center of transition metal compounds is highly susceptible to strain effects, thereby enabling the modulation of the hydrogen adsorption thermodynamics on strained solid surfaces. This insight is crucial for the design of materials with tailored properties for applications, such as catalysis and energy storage.

The flash Joule heating (FJH) method represents a novel approach to material synthesis, characterized by the induction of nonequilibrium, extremely high temperatures through rapid Joule heating, which also introduces strain, dislocations, and twins into an electrocatalyst.[22] The FJH method has been successfully exploited for various applications such as the synthesis of single atoms,[23] high-entropy alloys (HEA),[24] oxides,[25] and sulfides,[26] showing great potential for expedited and straightforward material fabrication. The strain effect engendered by the presence of twins and dislocations serves to optimize the electronic structure of the catalyst, thereby enhancing its catalytic activity.[27]

Herein, we demonstrate a rational design strategy for engineering twins within a lattice-matched Co/CoO heterostructure via Joule heating. By leveraging the homogeneous space group between Co and CoO, we achieve controllable twin boundary construction through oxygen incorporation under nonequilibrium conditions. The rapid cooling process effectively traps the interfacial strain induced by the lattice mismatch, leading to extensive atomic displacement from equilibrium positions, as confirmed by XAFS analysis. This strain engineering approach fundamentally modulates the electronic structure by downshifting the d-band center by 0.4 eV and flattening bands near the Fermi level, thereby optimizing the hydrogen binding energy and charge transfer kinetics. As a result, the engineered heterostructure achieves exceptional HER performance with an ultralow overpotential of 49.1 mV at 10 mA cm^{-2} and remarkable long-term stability exceeding 500 h. More significantly, when coupled with RuO_2, it enables industrial-level water splitting (1 A cm^{-2}) at a notably low cell voltage of 2.05 V. This work not only demonstrates an effective approach for boosting electrocatalytic activity through twin engineering but also provides fundamental insights into structure−activity relationships in transition metal-based catalysts.

The synthesis strategy for engineering a lattice-matched Co/CoO heterostructure is schematically illustrated in Figure 1a. The Co/CoO catalyst is fabricated via flash Joule heating (FJH), where oxygen molecules from the air are strategically incorporated into the metal lattice under nonequilibrium conditions. Due to the inherent lattice mismatch between Co and CoO, the rapid thermal shock and subsequent cooling process effectively trap significant interfacial strain energy. As depicted in Figure 1b, this localized stress induces plastic deformation in Co nanoparticles, triggering the formation of

https://doi.org/10.1021/acs.nanolett.5c00472
Nano Lett. XXXX, XXX, XXX−XXX

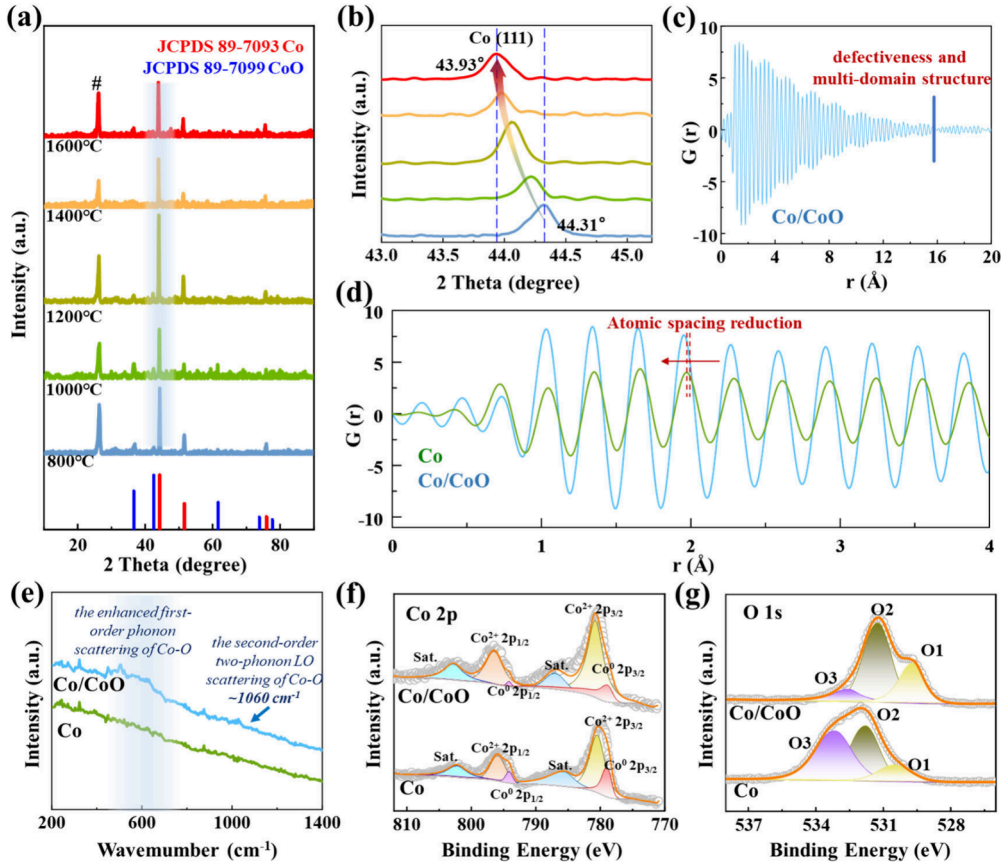

Figure 3. (a) XRD patterns of Co/CoO prepared at different temperatures (b) XRD patterns indexed to (111) diffraction planes of Co, extracted from (a). (c, d) PDF analysis of Co/CoO and Co. (e) Raman spectra of Co/CoO and Co. XPS survey spectra of Co/CoO and Co: (f) Co 2p; (g) O 1s.

extensive twin boundaries. The trapped strain fundamentally modulates the electronic structure by downshifting the d-band center, thereby optimizing the hydrogen adsorption energy for enhanced catalytic activity. The synthesized nanosheets (thickness <20 nm) uniformly coat carbon cloth fibers (Figure 1c), with no significant damage to morphology or conductivity after the FJH treatment (Figures S1−S4). TEM images (Figure 2d,e) reveal distinct fringes for Co at approximately 0.204 and 0.177 nm, corresponding to the (111) and (200) crystal planes, respectively. Similarly, CoO displays fringes at around 0.244 and 0.212 nm for the (111) and (200) planes, respectively. Oxidation to varying extents is observed around the periphery of Co grains, with these regions being identified as CoO. As illustrated in Figure 1f, significant lattice distortions are evident, encompassing atomic displacements from the regular lattice sites and slip (twinning). Selected area electron diffraction (SAED) patterns confirm the crystallinity of both Co and CoO (Figure 1g). Furthermore, the energy dispersive spectroscopy (EDS) elemental mapping images (Figure 1h) exhibit a distribution of Co, O, and C elements. Oxygen shows a uniform distribution across the particles, yet its mapping intensity is marginally lower than that of cobalt, indicating that it does not entirely cover the surface of the Co crystals.

The unique lattice-matched design enables extensive lattice distortion by leveraging the homogeneous space group between Co and CoO ($Fm\bar{3}m$, No. 225). High-resolution transmission electron microscopy (HRTEM) analysis (Figure 2a) directly visualizes the interface structure, where oxygen incorporation leads to controlled CoO formation while maintaining the crystallographic coherency. The inherent lattice constant mismatch between Co and CoO generates significant interfacial stress throughout the grains. This stress manifests as horizontal shear strain, resulting in the formation of symmetric twin boundaries along the (200) plane, as evidenced by HRTEM images (Figure 3b,c). The fast Fourier transform (FFT) image also exhibits two symmetric sets of spots, confirming the formation of twin crystals. Figure 3d,e display geometric phase analysis (GPA) images, which reveal minimal stresses along the vertical *y*-axis but significant strains along the horizontal *x*-axis and shear strains. In contrast, the Co sample is prepared under vacuum conditions, exhibiting a nanosheet morphology similar to that of Co/CoO (Figure S9). As depicted in Figure 2f, subsequent thermal treatment of the specimen in air facilitated the uniform deposition of CoO on the surface of Co (denoted as CoO@Co), with no discernible twinning observed at the interface. This observation suggests that conventional surface oxidation is not conducive to the formation of twin structures at the interface. Notably, transient high-temperature thermal shocks under nonequilibrium conditions are instrumental in inducing the formation of Co/CoO lattice-matched twins. Subsequently, X-ray absorption spectroscopy was employed to discern the chemical states of Co within the heterostructures. The K-edge is examined for shifts in the absorption threshold along the arrow, indicating an increase in the valence state. Notably, the observed valence state of cobalt in the sample appears to be intermediate between that of the pristine metallic cobalt (Co foil) and the

https://doi.org/10.1021/acs.nanolett.5c00472
Nano Lett. XXXX, XXX, XXX−XXX

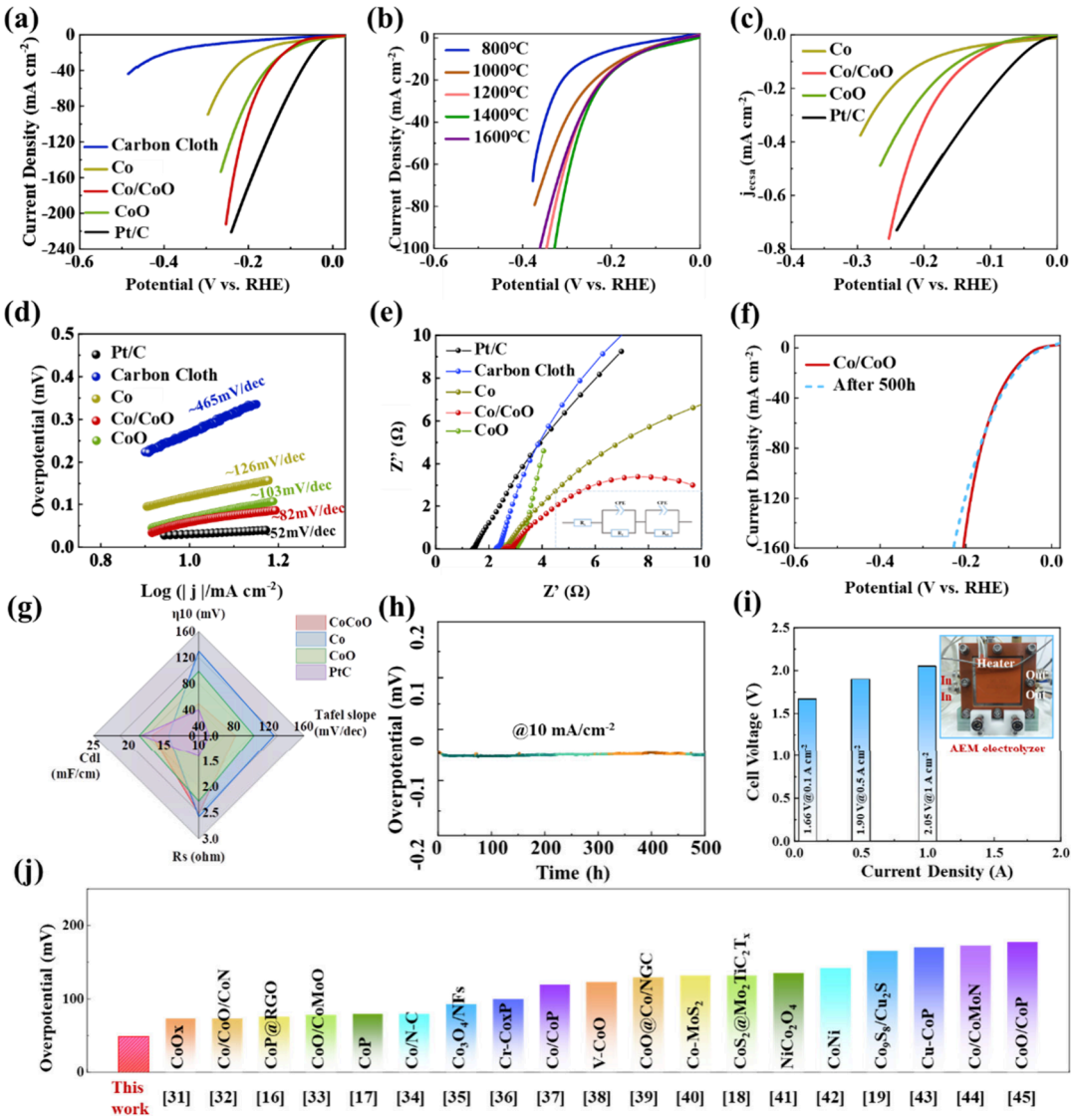

Figure 4. Electrocatalytic activities of Co/CoO toward hydrogen evolution reaction (HER). (a) LSV curves. (b) LSV curves at different temperatures. (c) LSV curves normalized by ECSA. (d) Tafel plots. (e) EIS spectra. (f) LSV after 500 h durability test. (g) Radar diagram of some key HER activity metrics of different catalysts. (h) Chronoamperometric curve recorded on Co/CoO at 10 mA cm^{-2}. (i) Photo diagram of AEM electrolyzer operation. (j) Performance comparison for our work and other similar electrocatalysts reported.

oxidized form CoO. The local atomic structure was then revealed through analysis of the Fourier-transformed (FT) extended X-ray absorption fine spectrum (EXAFS). The radial distribution function (R-space), in conjunction with the fitting results, predominantly exhibited Co−O and Co−Co coordination environments within the sample, corroborating the coexistence of elemental Co and CoO. A detailed comparison of the fitting data reveals a significant decrease in the coordination number of Co−Co in the sample relative to the benchmark sample, while the coordination distance remains unchanged. This observed decrease in coordination number may be associated with the occurrence of lattice distortion, suggesting that many atoms have deviated from their equilibrium positions within the crystalline lattice. As shown in Figure S12, the fitting curve matches the experimental curve very well, indicating that the results in the aforementioned table are true and reliable. The specific coordination numbers and other parameters are listed in Table S1.

The X-ray diffraction patterns of all samples match those of JCPDS cards 89-7093 (Co) and 89-7099 (CoO) (Figure 3a), with tensile strain increasing proportionally to thermal input. Higher-magnification analysis at 44° reveals a 0.38° leftward shift of the Co(111) crystal plane (Figure 3b). This shift stems from CoO formation within the homogeneous space group, as incorporated oxygen atoms expand the cobalt lattice. The precise control of oxidation level and resultant strain through current modulation leads to an optimized electronic structure, enhancing hydrogen adsorption−desorption kinetics and overall catalytic performance. Pair distribution function (PDF) analysis indicates smaller grain sizes than observed by TEM (Figure 3c), reflecting the defect-rich, multidomain nature of Co/CoO nanosheets. The PDF profile shows a leftward shift for Co/CoO compared with Co (Figure 3d), confirming reduced interatomic spacing from oxygen incorporation. Raman spectroscopy reveals enhanced first-order phonon scattering, typically forbidden in NaCl-type structures, suggesting structural defects and cobalt vacancies. A character-

https://doi.org/10.1021/acs.nanolett.5c00472
Nano Lett. XXXX, XXX, XXX−XXX

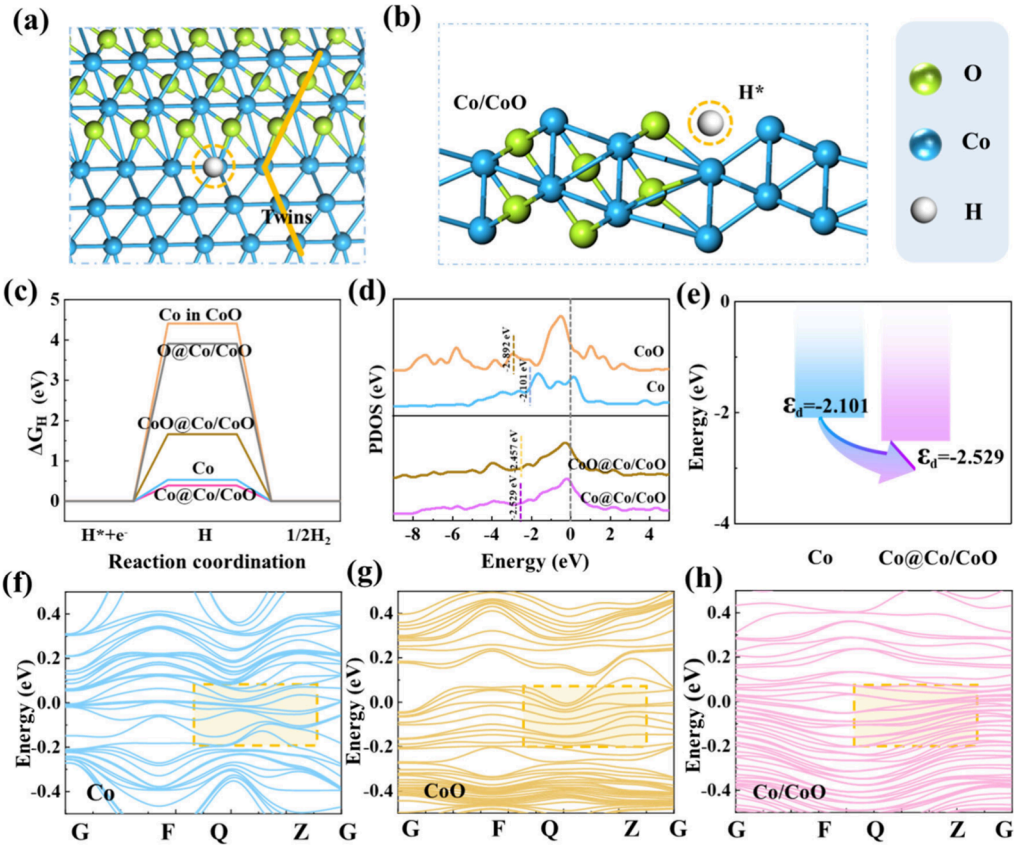

Figure 5. Theoretical calculation results of Co/CoO. (a, b) Atomic model of matched interface. (c) Free energy diagram of the HER for different adsorption sites. (d) PDOS with calculated Co d-band centers of Co in pure CoO, pure Co, Co of Co, Co of Co/CoO, and CoO of Co/CoO. (e) d-band centers of pure Co and Co of Co/CoO. The electronic energy band structure: (f) Co; (g) Co@Co/CoO; (h) CoO@Co/CoO.

istic second-order LO peak appears at ~1060 cm^{-1}.[28,29] XPS tests are performed to analyze the valence states and electronic structure. For Co 2p spectra (Figure 3f), a pronounced shift toward higher binding energy in the Co/CoO system, in contrast to the Co sample counterpart, implies a reduction in electron density at the cobalt sites. This observation is indicative of charge transfer occurring between the cobalt and oxygen constituents.[17] The oxygen content (Figure 3g) within the lattice, denoted as O1, exhibits a significant increase, corroborating the formation of CoO crystallizing in the same space group.[30] The more distinct O2 peak and EPR (Figure S14) spectra also indicate that the thermal shock method has successfully introduced oxygen vacancies while fabricating the nanosheet structure.

The LSV curves of Co/CoO nanosheets, Co nanosheets, CoO@Co, Pt/C, and pristine carbon cloth are shown in Figure 4a. Co/CoO nanosheets show superior activity with the lowest overpotentials (49.1 mV at 10 mA/cm^2). The optimal sample was obtained at 1400 °C (Figure 4b). As shown in Figure 4c, the normalized LSV curves show that the Co/CoO catalyst demonstrates superior intrinsic activity compared to Pt/C and other controls, confirming the high catalytic efficiency of the Co/CoO interface. As shown in Figure 4d, it is noted that the Tafel slopes exhibited the lowest of ~82 mV dec^{-1} which indicated that the formation of well-matched lattice structures is beneficial to the promotion of the kinetics of the HER reaction and thus improved the performance of the HER. EIS spectra reveal that Co/CoO nanosheet arrays display the smallest semicircle radius (Figure 4e), suggesting minimal charge transfer resistance and superior reaction kinetics. To determine the operational stability of the resulting samples, HER stability measurements are performed on the best samples at 1400 °C for up to 500 h at 10 mA cm^{-2}. The radar chart visually highlights the superior performance of the Co/CoO catalyst in terms of lower overpotential and Tafel slope as well as comparable or better electrochemical properties compared to the other catalysts (Figure 4g). As shown in Figure 4h, the catalyst electrodes exhibited consistent potential curves and displayed no significant decay in overpotentials, demonstrating excellent electrochemical stability. The electrochemical, morphological, structural, and compositional properties (Figure 4g) demonstrate the remarkable long-term durability of the Co/CoO heterostructure catalyst, affirming its potential for practical applications in alkaline water electrolysis. Under harsh industrial conditions (80 °C and 6 M KOH), the Co/CoO|| RuO_2 electrode pair demonstrates remarkable electrocatalytic performance, achieving a current density of 1 A cm^{-2} at an exceptionally low cell voltage of 2.05 V (Figure 4i), highlighting its potential for practical hydrogen production. A comparative analysis of hydrogen evolution reaction performance among analogous material systems reported over the past five years (Figure 4j) demonstrates that the lattice-matched Co/CoO heterostructure surpasses the majority of contemporary electrocatalysts.[16−19,31−45]

To reveal the nature of the heterojunction's role in boosting HER performance, we conducted DFT calculations and identified optimal H adsorption sites in the heterostructure

https://doi.org/10.1021/acs.nanolett.5c00472
Nano Lett. XXXX, XXX, XXX−XXX

model, as depicted in Figure 5a,b and Figure S18. Figure 5c illustrates a reduction in the Co site energy from 0.53 to 0.38 eV, and notably, the Co site within CoO decreases from 4.4 to 1.6 eV. This significant energy modulation originates from the interfacial strain induced by lattice matching (Figure 2d), which optimizes the electronic structure for HER catalysis. Further analysis via projected overlap density of states (PDOS) calculations elucidates the pivotal role of the matched interface in augmenting the hydrogen evolution reaction (HER). The electronic structures of Co at different sites benefit from tensile or compressive strain, which could be the origin of the weakened hydrogen adsorption free energy, and thus, HER activity is improved. As detailed in Figure 5d,e, the d-band center of the Co@Co/CoO site shifts away from the Fermi level. This shift improves the adsorption of hydrogen. The heightened electronic density of states at the CoO@Co/CoO interface across the Fermi level facilitates an enhancement of the electrical conductivity, which is advantageous for catalytic performance. Figure S28 demonstrates that the electrons around Co centers decrease while those around the O centers increase. Accordingly, the average valence of Co atoms becomes higher resulting from the introduction of O atoms, which is consistent with XPS analysis in Figure 3f. Band structure analysis (Figures 5f–h) reveals minimal dispersion near the Fermi level, indicating a high density of states and low electron momentum change. At the same time, the matched interface induces a flattening of the CoO bands, thereby enhancing the density of states near the Fermi level.

In summary, we have developed a flash Joule heating strategy to engineer twins within lattice-matched Co/CoO heterostructure through controlled oxygen incorporation under nonequilibrium conditions. Taking advantage of the homogeneous space group between Co and CoO, we achieve coherent twinning interfaces with trapped strain, as evidenced by significantly reduced Co coordination numbers in the XAFS analysis. The trapped interfacial strain fundamentally modulates the electronic structure, leading to a 0.4 eV downshift of the d-band center and flattened bands near the Fermi level, thereby optimizing the hydrogen binding energy and charge transfer kinetics. This rational design results in exceptional HER performance with an ultralow overpotential of 49 mV at 10 mA cm^{-2} and remarkable stability over 500 h. More importantly, when paired with RuO_2, the catalyst enables industrial-level water splitting at 1 A cm^{-2} with a notably low cell voltage of 2.05 V. These findings establish a fundamental understanding of twin engineering in electrocatalysts and demonstrate its effectiveness in enhancing catalytic activity, providing new insights for the rational design of high-performance energy conversion materials.

■ ASSOCIATED CONTENT

Supporting Information

The Supporting Information is available free of charge at https://pubs.acs.org/doi/10.1021/acs.nanolett.5c00472.

Details of the synthesis method and electrochemical measurement, additional TEM and HRTEM images of catalysts, XPS survey spectra, fitting results of XAFS, comparison of HER catalytic performance, and computational simulations (PDF)

■ AUTHOR INFORMATION

Corresponding Authors

Junlei Qi − *State Key Laboratory of Precision Welding and Joining of Materials and Structure, Harbin Institute of Technology, Harbin 150001, China;* orcid.org/0000-0003-3367-1241; Email: jlqi@hit.edu.cn

Shude Liu − *Engineering Research Center of Technical Textile, Ministry of Education, College of Textiles, Donghua University, Shanghai 201620, China;* orcid.org/0000-0001-8983-2097; Email: sdliu@dhu.edu.cn

Ling Kang − *School of Mechanical Engineering, Yonsei University, Seoul 120-749, South Korea;* orcid.org/0000-0001-6515-464X; Email: 52171213015@stu.ecnu

Yaotian Yan − *State Key Laboratory of Precision Welding and Joining of Materials and Structure, Harbin Institute of Technology, Harbin 150001, China*; Email: ytyanhit@hit.edu.cn

Authors

Taili Yang − *State Key Laboratory of Precision Welding and Joining of Materials and Structure, Harbin Institute of Technology, Harbin 150001, China*

Ruonan Liu − *State Key Laboratory of Precision Welding and Joining of Materials and Structure, Harbin Institute of Technology, Harbin 150001, China*

Keke Huang − *State Key Laboratory of Precision Welding and Joining of Materials and Structure, Harbin Institute of Technology, Harbin 150001, China*

Rongrong Xu − *State Key Laboratory of Precision Welding and Joining of Materials and Structure, Harbin Institute of Technology, Harbin 150001, China*

Jiping Chen − *State Key Laboratory of Precision Welding and Joining of Materials and Structure, Harbin Institute of Technology, Harbin 150001, China*

Jinchun Tu − *State Key Laboratory of Marine Resource Utilization in South China Sea, College of Materials and Chemical Engineering, Hainan University, Haikou 570228, China*

Zixuan Wang − *Institute of Intelligent Ocean Engineering, Harbin Institute of Technology (Shenzhen), Shenzhen 518055, China*

Jian Cao − *State Key Laboratory of Precision Welding and Joining of Materials and Structure, Harbin Institute of Technology, Harbin 150001, China*

Complete contact information is available at: https://pubs.acs.org/10.1021/acs.nanolett.5c00472

Notes

The authors declare no competing financial interest.

■ ACKNOWLEDGMENTS

This work was supported by the National Natural Science Foundation of China (Grant No. 52175303), the National Science Fund for Distinguished Young Scholars (Grant No. 52125502), the Postdoctoral Fellowship Program of CPSF under Grant Number GZB20240949, Natural Science Foundation of Heilongjiang Province (LH2024E031), Heilongjiang Postdoctoral Fund (LBH-Z24174), Key Research and Development Project of Hainan Province (ZDYF2024SHFZ082), State Key Laboratory of Precision Welding & Joining of Materials and Structures (24-R-01 and 24-Z-07), Guangdong Provincial Natural Science Foundation

https://doi.org/10.1021/acs.nanolett.5c00472
Nano Lett. XXXX, XXX, XXX−XXX

General Program (Grant No. 2024A1515011319) and Guangdong Province Basic and Applied Basic Research Fund Joint Fund - Youth Fund project (Grant No. 2023A1515110653). Special thanks to HIT Center of Analysis Measurement and Computing and Dr. Zheng Zhen for the electron microscope test analysis. Special thanks for the support of Suzhou XZX Hydrogen Energy Technology Co., Ltd. The authors gratefully acknowledge the support of bottled purified water from Hangzhou Wahaha Group Co., Ltd.

REFERENCES

(1) Li, A.; Kong, S.; Adachi, K.; Ooka, H.; Fushimi, K.; Jiang, Q.; Ofuchi, H.; Hamamoto, S.; Oura, M.; Higashi, K.; Kaneko, T.; Uruga, T.; Kawamura, N.; Hashizume, D.; Nakamura, R. Atomically dispersed hexavalent iridium oxide from MnO_2 reduction for oxygen evolution catalysis. *Science* **2024**, *384* (6696), 666−670.

(2) Zhou, S.; Shi, L.; Li, Y.; Yang, T.; Zhao, S. Metal-organic framework-based electrocatalysts for acidic water splitting. *Adv. Funct. Mater.* **2024**, *34*, 2400767.

(3) Liu, T.; Zhao, Z.; Tang, W.; Chen, Y.; Lan, C.; Zhu, L.; Jiang, W.; Wu, Y.; Wang, Y.; Yang, Z.; Yang, D.; Wang, Q.; Luo, L.; Liu, T.; Xie, H. In-situ direct seawater electrolysis using floating platform in ocean with uncontrollable wave motion. *Nat. Commun.* **2024**, *15*, 5305.

(4) Zhang, C.; Qin, S.; Gao, H.; Jin, P. High hydrogen evolution activities of dual-metal atoms incorporated N-doped graphenes achieved by coordination regulation. *J. Mater. Inf.* **2024**, *4*, 1.

(5) Hu, F.; Yu, D.; Ye, M.; Wang, H.; Hao, Y.; Wang, L.; Li, L.; Han, X.; Peng, S. Lattice-matching formed mesoporous transition metal oxide heterostructures advance water splitting by active Fe−O−Cu bridges. *Adv. Energy Mater.* **2022**, *12*, 2200067.

(6) Shi, Y.; Ma, Z. R.; Xiao, Y. Y.; Yin, Y. C.; Huang, W. M.; Huang, Z. C.; Zheng, Y. Z.; Mu, F. Y.; Huang, R.; Shi, G. Y.; Sun, Y. Y.; Xia, X. H.; Chen, W. Electronic metal-support interaction modulates single-atom platinum catalysis for hydrogen evolution reaction. *Na.t Commun.* **2021**, *12*, 3021.

(7) Guo, B.; Ding, Y.; Huo, H.; Wen, X.; Ren, X.; Xu, P.; Li, S. Recent advances of transition metal basic salts for electrocatalytic oxygen evolution reaction and overall water electrolysis. *Nano-Micro Lett.* **2023**, *15*, 57.

(8) Rekha, P.; Yadav, S.; Singh, L. A review on cobalt phosphate-based materials as emerging catalysts for water splitting. *Ceram. Int.* **2021**, *47*, 16385−16401.

(9) Jia, Y.; Li, Y.; Zhang, Q.; Yasin, S.; Zheng, X.; Ma, K.; Hua, Z.; Shi, J.; Gu, C.; Dou, Y.; Dou, S. Deactivation mechanism for water splitting: Recent advances. *Carbon Ener* **2024**, *6*, No. e528.

(10) Wang, C.; Zhang, Q.; Yan, B.; You, B.; Zheng, J.; Feng, L.; Zhang, C.; Jiang, S.; Chen, W.; He, S. Facet engineering of advanced electrocatalysts toward hydrogen/oxygen evolution reactions. *Nano-Micro Lett.* **2023**, *15*, 52.

(11) Zeng, S.; Shi, H.; Dai, T.; Liu, Y.; Wen, Z.; Han, G.; Wang, T.; Zhang, W.; Lang, X.; Zheng, W.; Jiang, Q. Lamella-heterostructured nanoporous bimetallic iron-cobalt alloy/oxyhydroxide and cerium oxynitride electrodes as stable catalysts for oxygen evolution. *Nat. Commun.* **2023**, *14*, 1811.

(12) Zeng, Y.; Zhao, M.; Huang, Z.; Zhu, W.; Zheng, J.; Jiang, Q.; Wang, Z.; Liang, H. Surface reconstruction of water splitting electrocatalysts. *Adv. Energy Mater.* **2022**, *12*, 2201713.

(13) Anantharaj, S.; Noda, S.; Jothi, V. R.; Yi, S.; Driess, M.; Menezes, P. W. Strategies and perspectives to catch the missing pieces in energy-efficient hydrogen evolution reaction in alkaline media. *Angew. Chem. Int. Ed* **2021**, *60*, 18981−19006.

(14) Tang, T.; Ding, L.; Yao, Z. C.; Pan, H. R.; Hu, J. S.; Wan, L. J. Synergistic electrocatalysts for alkaline hydrogen oxidation and evolution reactions. *Adv. Funct. Mater.* **2022**, *32*, 2107479.

(15) Zhu, Y.; Wang, J.; Koketsu, T.; Kroschel, M.; Chen, J.; Hsu, S.; Henkelman, G.; Hu, Z.; Strasser, P.; Ma, J. Iridium single atoms incorporated in Co_3O_4 efficiently catalyze the oxygen evolution in acidic conditions. *Nat. Commun.* **2022**, *13*, 7754.

(16) Luo, Y.; Wang, P.; Zhang, G.; Wu, S.; Chen, Z.; Ranganathan, H.; Sun, S.; Shi, Z. Mn-doped nickel−iron phosphide heterointerface nanoflowers for efficient alkaline freshwater/seawater splitting at high current densities. *Chem. Eng. J.* **2023**, *454*, 140061.

(17) Yang, T.; Xie, H.; Ma, N.; Liu, E.; Shi, C.; He, C.; Zhao, N. Unraveling the mechanism of hydrogen evolution reaction on cobalt compound electrocatalysts. *Appl. Surf. Sci.* **2021**, *550*, 149355.

(18) Chen, X.-L.; Liu, C.; Tang, C.-K.; Liu, Z.-H.; Lü, Q.-F.; Jin, Y. CoS_2 nanoparticles grown on $Mo_2TiC_2T_x$ as an efficient electrocatalyst for hydrogen evolution reaction. *Diam. Relat. Mater.* **2023**, *135*, 109877.

(19) Zhu, C.; Wang, A. L.; Xiao, W.; Chao, D.; Zhang, X.; Tiep, N. H.; Chen, S.; Kang, J.; Wang, X.; Ding, J.; Wang, J.; Zhang, H.; Fan, H. J. In situ grown epitaxial heterojunction exhibits high-performance electrocatalytic water splitting. *Adv. Mater.* **2018**, *30*, 1705516.

(20) Song, W.; Li, M.; Wang, C.; Lu, X. Electronic modulation and interface engineering of electrospun nanomaterials-based electrocatalysts toward water splitting. *Carbon Ener* **2021**, *3*, 101−128.

(21) Ye, L.; Chen, W.; Jiang, Z.; Jiang, Z. Co/CoO heterojunction rich in oxygen vacancies introduced by O_2plasma embedded in mesoporous walls of carbon nanoboxes covered with carbon nanotubes for rechargeable zinc−air battery. *Carbon Ener* **2024**, *6*, No. e457.

(22) Hu, X.; Zuo, D.; Cheng, S.; Chen, S.; Liu, Y.; Bao, W.; Deng, S.; Harris, S. J.; Wan, J. Ultrafast materials synthesis and manufacturing techniques for emerging energy and environmental applications. *Chem. Soc. Rev.* **2023**, *52*, 1103−1128.

(23) Xing, L.; Liu, R.; Gong, Z.; Liu, J.; Liu, J.; Gong, H.; Huang, K.; Fei, H. Ultrafast Joule heating synthesis of hierarchically porous graphene-based Co-N-C single-atom monoliths. *Nano Res.* **2022**, *15*, 3913−3919.

(24) Cha, J. H.; Cho, S. H.; Kim, D. H.; Jeon, D.; Park, S.; Jung, J. W.; Kim, I. D.; Choi, S. Y. Flash-thermal shock synthesis of high-entropy alloys toward high-performance water splitting. *Adv. Mater.* **2023**, *35*, 2305222.

(25) Yan, Y.; Lin, J.; Huang, K.; Zheng, X.; Qiao, L.; Liu, S.; Cao, J.; Jun, S. C.; Yamauchi, Y.; Qi, J. Tensile Strain-Mediated Spinel Ferrites Enable Superior Oxygen Evolution Activity. *J. Am. Chem. Soc.* **2023**, *145*, 24218−24229.

(26) Wu, H.; Lu, Q.; Zhang, J.; Wang, J.; Han, X.; Zhao, N.; Hu, W.; Li, J.; Chen, Y.; Deng, Y. Thermal shock-activated spontaneous growing of nanosheets for overall water splitting. *Nanomicro Lett.* **2020**, *12*, 1−12.

(27) Zhang, W.; Liu, M.; Gu, X.; Shi, Y.; Deng, Z.; Cai, N. Water electrolysis toward elevated temperature: advances, challenges and frontiers. *Chem. Rev.* **2023**, *123*, 7119−7192.

(28) Li, Y.; Qiu, W.; Qin, F.; Fang, H.; Hadjiev, V. G.; Litvinov, D.; Bao, J. Identification of cobalt oxides with raman scattering and fourier transform infrared spectroscopy. *J. Phys. Chem. C* **2016**, *120*, 4511−4516.

(29) Rivas-Murias, B.; Salgueiriño, V. Thermodynamic CoO−Co_3O_4 crossover using raman spectroscopy in magnetic octahedron-shaped nanocrystals. *J. Raman Spectrosc.* **2017**, *48*, 837−841.

(30) Have, I. C. T.; Kromwijk, J. J. G.; Monai, M.; Ferri, D.; Sterk, E. B.; Meirer, F.; Weckhuysen, B. M. Uncovering the reaction mechanism behind CoO as active phase for CO_2 hydrogenation. *Nat. Commun.* **2022**, *13*, 324.

(31) Feng, J.; Qiao, L.; Zhou, P.; Bai, H.; Liu, C.; Leong, C.; Chen, Y.; Fai, W.; Ni, J.; Pan, H. Nanocrystalline CoO_x glass for highly-efficient alkaline hydrogen evolution reaction. *J. Mater. Chem. A* **2022**, *11*, 316−329.

(32) Zhang, W.; Li, C.; Ji, J.-Y.; Niu, Z.; Gu, H.; Abrahams, B. F.; Lang, J.-P. Tailorable carbon cloth electrodes covered with heterostructured Co/CoO/CoN interfaces for scalable electrocatalytic overall water splitting. *Chem. Eng. J.* **2023**, *461*, 141937.

(33) Bian, H.; Chen, Z.; Chen, T.; Humayun, M.; Zhou, B.; Liao, W.; Li, Z.; Zhang, Z.; Wang, C.; Liu, C. Anodically designing of

https://doi.org/10.1021/acs.nanolett.5c00472
Nano Lett. XXXX, XXX, XXX−XXX

refreshable bi-metallic oxides for highly-efficient hydrogen evolution. *Chem. Eng. J.* **2023**, *466*, 143045.
(34) Dang, J.; Yun, S.; Zhang, Y.; Yang, J.; Liu, Z.; Dang, C.; Wang, Y.; Deng, Y. Constructing double-shell structured N-C-in-Co/N-C electrocatalysts with nanorod- and rhombic dodecahedron-shaped hollow morphologies to boost electrocatalytic activity for hydrogen evolution and triiodide reduction reaction. *Chem. Eng. J.* **2022**, *449*, 137854.
(35) Wang, T.; Shi, Y.; Fei, J.; Zhu, J.; Song, L.; Li, C.; Zhan, T.; Lai, J.; Wang, L. Three-dimensional interconnected nanofibers consisting of ultra-small Ni-doped Co_3O_4 nanoparticles for acidic overall water splitting at high current density. *Appli. Catal. B Environ.* **2024**, *358*, 124367.
(36) Song, Y.; Sun, M.; Zhang, S.; Zhang, X.; Yi, P.; Liu, J.; Huang, B.; Huang, M.; Zhang, L. Alleviating the Work Function of Vein-Like Co_XP by Cr Doping for Enhanced Seawater Electrolysis. *Adv. Funct. Mater.* **2023**, *33*, 2214081.
(37) Li, W.; Liu, J.; Guo, P.; Li, H.; Fei, B.; Guo, Y.; Pan, H.; Sun, D.; Fang, F.; Wu, R. Co/CoP heterojunction on hierarchically ordered porous carbon as a highly efficient electrocatalyst for hydrogen and oxygen evolution. *Adv. Energy Mater.* **2021**, *11*, 2102134.
(38) He, J.; Liu, F.; Chen, Y.; Liu, X.; Zhang, X.; Zhao, L.; Chang, B.; Wang, J.; Liu, H.; Zhou, W. Cathode electrochemically reconstructed V-doped CoO nanosheets for enhanced alkaline hydrogen evolution reaction. *Chem. Eng. J.* **2022**, *432*, 134331.
(39) Gu, L.; Chen, J.; Zhou, T.; Lu, X.; Li, G. Engineering cobalt oxide by interfaces and pore architectures for enhanced electrocatalytic performance for overall water splitting. *Nanoscale* **2020**, *12*, 11201.
(40) Doan, T. L. L.; Nguyen, D. C.; Prabhakaran, S.; Kim, D. H.; Tran, D. T.; Kim, N. H.; Lee, J. H. Single-atom Co-decorated MoS_2 nanosheets assembled on metal nitride nanorod arrays as an efficient bifunctional electrocatalyst for pH-universal water splitting. *Adv. Funct. Mater.* **2021**, *31*, 2100233.
(41) Zhang, Z.; Liu, X.; Wang, D.; Wan, H.; Zhang, Y.; Chen, G.; Zhang, N.; Ma, R. Ruthenium composited $NiCo_2O_4$ spinel nanocones with oxygen vacancies as a high-efficient bifunctional catalyst for overall water splitting. *Chem. Eng. J.* **2022**, *446*, 137037.
(42) Zhang, T.; He, Z.; Yin, L.; Gao, W.; Wang, Y. CoNi alloy nanoparticles confined by N-doped carbon matrix with tailored d-Band center for electrocatalytic hydrogen evolution. *Fuel* **2024**, *365*, 131176.
(43) Zou, L.; Wei, Y.-S.; Wang, Q.; Liu, Z.; Xu, Q.; Kitagawa, S. Cobalt phosphide nanofibers derived from metal-organic framework composites for oxygen and hydrogen evolutions. *Sci. China Mater.* **2023**, *66*, 3139−3145.
(44) Ma, H.; Chen, Z.; Wang, Z.; Singh, C. V.; Jiang, Q. Interface Engineering of Co/CoMoN/NF Heterostructures for high-performance electrochemical overall water splitting. *Adv. Sci.* **2022**, *9*, 2105313.
(45) Chen, K.; Cao, Y.; Wang, W.; Diao, J.; Park, J.; Dao, V.; Kim, G.-C.; Qu, Y.; Lee, I.-H. Effectively enhanced activity for overall water splitting through interfacially strong P−Co−O tetrahedral coupling interaction on CoO/CoP heterostructure hollow-nanoneedles. *J. Mater. Chem. A* **2023**, *11*, 3136−3147.

https://doi.org/10.1021/acs.nanolett.5c00472
Nano Lett. XXXX, XXX, XXX−XXX